Numerical prediction of breast skin temperature based on thermographic and ultrasonographic data in healthy and cancerous breasts

Q1 Ilona Korczak [a,*], Agnieszka Romowicz [b], Barbara Gambin [a], Tadeusz Palko [b], Eleonora Kruglenko [a], Katarzyna Dobruch-Sobczak [a]

[a] Institute of Fundamental Technological Research of the Polish Academy of Sciences, 02-106 Warsaw, Pawinskiego 5B, Poland
[b] Institute of Metrology and Biomedical Engineering Faculty of Mechatronics of the Warsaw University of Technology, 02-525 Warsaw, Sw. Andrzeja Boboli 8, Poland

ARTICLE INFO

ABSTRACT

Breast cancer is one of the most common women's cancers, so an available diagnostic modality, particularly non-invasive, is important. Infrared thermography (IRT) is a supporting diagnostic modality. Until now, many finite element methods (FEM) numerical models have been constructed to evaluate IRT's diagnostic value and to relate breast skin temperature characteristics with breast structural disorder presence, particularly to distinguish between cancerous types and normal structures. However, most of the models were not based on any clinical data, except for several papers based on clinical magnetic resonance imaging (MRI) data, wherein a three-dimensional (3D) breast model was studied. In our paper, we propose a very simplified numerical two-dimensional FEM model constructed based on clinical ultrasound data of breasts, which is much cheaper and available in real-time as opposed to MRI data. We show that our numerical simulations enabled us to distinguish between types of healthy breasts in agreement with the clinical classification and with thermographic results. The numerical breast models predicted the possibility of differentiation of cancerous breasts from healthy breasts by significantly different skin temperature variation ranges. The thermal variations of cancerous breasts were in the range of 0.5 °C–3.0 °C depending on the distance of the tumor from the skin surface, its size, and the cancer type. The proposed model, due to its simplicity and the fact that it was constructed based on clinical ultrasonographic data, can compete with the more sophisticated 3D models based on MRI.

© 2020 Published by Elsevier B.V. on behalf of Nalecz Institute of Biocybernetics and Biomedical Engineering of the Polish Academy of Sciences.

1. Introduction

Breast cancer is one of the most common cancers in women all over the world. In Poland, until 2007, breast cancer was the most common cause of all cancer-related deaths affecting the female population; now, it is in second place after lung cancer [1].The etiology of breast cancer is unknown. Undoubtedly, one of the most important risk factors of breast cancer with high penetration is the mutation of the tumor suppressor genes named *BRCA1* and *BRCA2*. The standard techniques of diagnostic imaging of breast cancer are mammography, magnetic resonance imaging (MRI), positron emission tomography (PET), and ultrasonography. Mammography is the most popular standard screening technique for the early detection of breast cancer. However, it is an invasive technique due to ionizing irradiation and is not friendly to patients because of examination discomfort, particularly for pregnant patients. Additionally, mammography is not recommended for dense breast study. However, noninvasive MRI and PET are time-consuming imaging techniques. Additionally, they need expensive equipment and are not readily available. They also require more qualified personnel to perform the examination.

A new technique that could help in the early diagnosis of breast cancer has been continuously sought. The review paper [2] discussed recent trends in novel microwave imaging (MI). The paper reviewed the current most commonly available screening methods and biomarkers along with biosensor techniques for diagnosing early-stage breast cancer. The authors stated that recent developments in the MI approaches and biosensors using different biomarkers for breast cancer detection have brought new hope for improvement of the diagnosis of early-stage breast cancer because MI has the potential to become a low-risk alternative or clinical complement to conventional mammography for diagnosing breast cancer. However, it should be underlined that MI and biosensor techniques are still not being implemented for clinical trials. Contrary to the above-discussed modalities, breast ultrasonography is already clinically acceptable, cheap, quick, safe, non-invasive, and the most accessible imaging technique [3]. However, the proper interpretation of ultrasound images, as opposed to imaging involving non-mechanical waves, is complicated and strongly dependent on the type of equipment and the doctor's experience, as proposed by [2]. Breast ultrasonography has been additionally enriched in recent years by parallel imaging of microflows (Doppler imaging) and imaging of local tissue stiffness as described in [4], but computer diagnosis instead of a doctor's diagnosis of breast cancer is still not acceptable. Additionally, researchers still continuously seek new modalities of ultrasonography (USG) useful in the early diagnosis of breast cancer or therapy monitoring, including chemotherapy [5].

The idea of evaluating breast tissue abnormalities by non-invasive registering of breast skin temperature, i.e. infrared thermography (IRT), appeared after advanced infrared thermometers began to be available. A major contribution in this field was described in papers [6–8], and a review paper [9], written by the same group of authors, presented the thermography as promising noninvasive breast tumor detection, as did the more recent review paper [10]. The authors developed a numerical finite element method (FEM) breast model with idealized three-dimensional geometry. The numerical breast model was built from tissue components (regions) such as the areola, subcutaneous fat layer, gland, muscle, thoracic wall, and tumor regions. The authors compared the results with the results obtained during IRT tests. Numerical simulation along with IRT results was used to estimate the metabolic heat production in [11] and [12]. In these papers, to prove the thesis that infrared imaging can be a useful tool to describe the malignancy of a tumor, a three-dimensional (3D) model of a breast was used in the FEM simulations. The numerical estimation of temperature distribution on breast skin by an idealized two-dimensional (2D) model of a breast was studied in many papers as proposed by [13], [14]. The geometry of the model of the breast was assumed as a 2D hemisphere shape, consisting of several layers similar to the symmetry and internal tissue structure of the mammary gland. The authors` studies focused on cancer size and location and its influence on surface temperature distribution. In [12] and [13], the effect of metabolism and the perfusion rate on the skin temperature profile was analyzed. The results showed that blood perfusion has a greater influence on the temperature distribution than the value of metabolism. In [15], the relationships between the location, size, and depth of a breast tumor and the heat-generation rate using the value of skin temperature distribution obtained from IRT were analyzed. The artificial neural network (ANN) and genetic algorithm were applied. In [16], an automatic algorithm named fuzzy active contours was created to segment the cancerous breast regions from thermography. The program could select the edges and core from the analyzed image of a tumor.

All of the abovementioned FEM models and many other models dealing with bioheat transfer inside breasts or other tissues are based on Penne's bioheat transfer equation proposed in [17], which is also used in our paper. Recently, in [18], thermographic images as an additional tool for early breast cancer detection were discussed. In the paper, a 2D model of a breast in the COMSOL software was used to estimate the temperature of the breast surface. The temperature distribution in the three main types of breast cancer and healthy breasts were compared without assuming the values of the breast tissue's thermophysical properties. The authors underlined that IRT could be a great additional diagnostic technique. Nowadays, the literature on that subject has also highlighted the great potential of thermography as an additional method in early breast cancer screening. In [19], the use of machine learning applied to the thermography of breast tissue for the early detection of breast cancer was proposed. The breast condition classification was carried out using two methods, namely ANN and support vector machines. In a recent paper [20], the role of IRT and the importance of numerical models in the further development of thermography were reviewed. Image acquisition protocols, segmentation techniques, feature extractions, and classification methods have been presented to increase the reliability of thermography over the years due to the development of machine learning and ANN. Particularly, in [21], the modern technique of machine learning was used to improve the reliability of thermography. Classification of breast screening

No.	The thickness of the fat layer [mm]	Distance between cyst and skin [mm]	Cyst radius [mm]	Type of breast
1	5.28	20.70	8.18	P2
2	7.45	14.70	3.00	P2
3	7.48	20.40	3.00	P1
4	3.66	0.00	0.00	N1

Table 1 – Characterization of the four healthy breasts.

IRT to passive and active was recently proposed in [22]. Passive screening does not use any additional energy supplied to the body of the test subject during temperature measurement. Active IRT uses the changes in the image of the temperature distribution that occur due to the introduction of external heating or cooling sources. In [22], different regimes of the external infrared radiation transmission regarded as the impact of infrared energy in reading dynamic thermography were analyzed. Additionally, cooling as an external stimulus introduced to breast IRT resolution enhancement was studied in [23] using commercial COMSOL FEM software. The authors demonstrated that the relationships between the temperature distributions obtained by computational modeling combined with thermographic imaging and dynamic cooling can be an important tool in the early detection of breast cancer. Numerical modeling of temperature distribution allows for elucidating the relationships between the process of internal temperature transfer in breast tissue and the temperature profile on its surface. Measuring the spatial temperature distribution inside the tissue in vivo necessary not only for diagnostic purposes but also for thermal therapy applications is one of the most important research issues. A good standard of internal temperature measurement is the MRI technique. For example, in high-intensity focused ultrasound therapies, the knowledge of the thermal dose and size of thermal lesions as well as, in diagnostic ultrasound imaging, the thermal state of the breast are crucial, so many numerical models of bioheat transfer were used and described in [24–26]. Other modern early cancer detection techniques, e.g. MI as proposed by [27,28], and photoacoustic imaging, as proposed by [29], also need numerical modeling support in the context of bioheat transfer. Recently, attention was paid in [30] to the fact that, in the IRT diagnosis of cancer, not only the breast gland but also the breast nodule should be taken into account. Modest but non-standard applications of estimation of the relationships between the spatial temperature distribution inside breast tissue and on its surface were considered in [31,32]. In those papers, it was shown that forced temperature changes inside the breast in vivo caused by heating the breast skin by several degrees Celsius improved the quality of ultrasound imaging.

In the following, we limited ourselves to take into account only passive thermography results. We also did not use sophisticated numerical modeling; we just aimed to show a simple idea of how, using standard breast ultrasonography together with a simplified model of bioheat transfer, we can predict the internal breast anatomical structure. We examined 14 women to confirm the thermography measurements in connection with an assessment of cancer diagnosis possibilities.

The paper is organized as follows. Section 2 describes the ultrasonic and IRT data acquisition and basic formulation of the FEM numerical breast bioheat transfer model. Section 3 summarizes the results, and Sections 4 and 5 contain the discussion and concluding remarks, respectively.

2. Materials and methods

We studied the healthy and cancerous breasts of 14 women. The ultrasound data for the healthy breasts were obtained by performing an ultrasound examination at the Institute of Fundamental Technological Research of the Polish Academy of Science. Informed consent was obtained from all patients participating in the study to performed examination and publish the report. The group of women with healthy breasts was represented only by four volunteers aged between 25 and 70 years. Due to the limited number of subjects, our investigation should be treated as a case study. It could help us frame questions for more rigorously designed clinical studies. Ultrasound examinations were performed according to Polish Ultrasounds Society standards, cf. [33], using UltrasonixSonix Touch machine with linear probe L5−14 MHz.The results obtained from the ultrasonography examination of the four healthy breasts are given in Table 1. The first column contains the calculated from ultrasonographic scans mean values of the breast tissue layers, the second and the third, the position and size of the cyst, respectively, and the fourth contains the breast density category, [34]. Namely, N1 corresponds to fatty normal breast, P1, and P2 to prominent ducts occupying less than 25%, and more than 25% but less than 75% of the breast volume, respectively.

The ultrasound data of the second breast group, cancerous breasts, was chosen from the medical database of breast cancer was created previously in the Institute of Fundamental Technological Research of the Polish Academy of Science, published in [35]. The database was reviewed and grouped for cases with cancer and concerning the tumor's size and location in the breast. The selection of cases for our analysis was guided by the assumption that the data were sufficiently diverse in terms of tumor size and distance from the surface of the breast skin. We limited ourselves to choosing 10 cases of breasts with cancer. Table 2 contains the results of the doctor's ultrasonography examination of the 10 cancerous breasts. The first two columns contain the width of the tissue layer calculated as mean values from ultrasonographic scans, and the next columns contain the tumor size and position. Similarly, as in Table 1, the width of tissue layers given in the two first columns, are calculated from ultrasonographic scans mean values, and the two next columns contain the cyst characteristics and type of breast.

At first, we introduced as simply as possible the geometrical model's usefulness for estimation of temperature distribution

No.	Skin layer [mm]	Fat layer [mm]	Tumor radius [mm]	Tumor coordinates E and C [mm]	
1	1.38	4.85	2.65	16.06	11.96
2	2.49	5.37	4.83	9.21	13.14
3	0.82	Not Applicable	3.80	16.60	27.23
4	1.44	Not Applicable	7.70	17.48	23.99
5	1.89	6.86	7.67	23.51	22.09
6	1.06	5.67	6.02	19.61	16.19
7	0.94	8.82	3.18	17.15	17.25
8	2.29	6.32	1.78	25.56	11.82
9	1.01	6.50	2.89	23.10	20.66
10	1.47	9.04	13.66	20.74	25.63

Table 2 – Characterization of 10 cancerous breasts.

on the breast skin surface of the healthy breasts and cancerous breasts. To this end, the ultrasound data from the US images of the 14 breasts were transferred to the MATLAB software (The MathWorks Inc., Natick, MA, U.S.A., version R2015a). Using the standard image analysis, we found the individual thickness of layers such as the skin, fat, and glandular layers. Additionally, the sizes of lesions, tumors, or cysts and their locations concerning the skin surface were determined. The obtained values were averaged and used as parameters in the geometrical breast model created as a 2D structure (Fig. 2) directly related to the USG scan. Based on the geometry presented in Fig. 2, the numerical modeling of bioheat transfer was performed in the AbaqusFEM software (Abaqus 6.11 software, Dassault SystèmesSimulia Corp., Providence, RI, U.S. A.). In the numerical simulation, a custom-developed program written in Fortran (Intel Visual Fortran Compiler Professional 11.1) to model perfusion and metabolism factors was used. The steps performed to compare the temperature distribution on the surface of the breasts obtained from the thermography images and temperature distributions calculated by the FEM models are presented in Fig. 1.

The thermographic examination was performed for the four healthy volunteers, at the company Braster SA using their thermography equipment, and the method described in [36]. During the test, the ambient temperature was 22 °C. Body temperature stabilization was achieved after one hour. The study was conducted in an air-conditioned room without windows. Before performing thermographic tests, each patient completed an appropriate questionnaire, taking into account information about the health condition and any reservations that would make it impossible to perform the experiment and exclude the patient from the examination. Before the procedure, the candidate was informed about the course of the examination. The patient had to give the written consent to perform a thermography test. Moreover, before the test was

forbidden to take any physical exertion, eat hot drinks and meals. The examination was performed in the sitting patient's position, face to the FLIR thermographic camera, the Therma-CAM^{TM} S45 model, which has a field of view of 24° x 18°/0.3 m, the spatial resolution of 1.3 mrad, type detector focal plane array (FPA), uncooled micro-bolometer, 320×240 pixels; a spectral range of 7.5–13 mm; temperature range used between - 10 °C and + 55 °C, the accuracy of 71% of readings. The test results were saved in a digital form on the computer disk. The obtained thermographic data was analyzed in the FLIR Research IR^{TM} Software program. An exemplary image of breast skin thermography is shown in Fig. 3. The mean temperatures of both the left and right breasts were determined. Furthermore, the points with the highest and the lowest temperatures were located.

The numerical simulations of the breasts were based on Penne's bioheat equation (see [17]).The effects of metabolism and blood perfusion were added as additional heat sources to the heat transfer equation in the heterogeneous volume of breast tissue. The following form of Penne's equation was used in the FEM simulations:

$$\rho_t(x)c_t(x)\frac{\partial T}{\partial t} = \nabla \cdot k_t(x)\nabla T + \rho_b c_b w_b(T_b - T) + Q_m(x) \text{ for x in V,} \qquad (1)$$

Where t denotes time, ($\cdot$) denotes the scalar multiplication of vectors, ∇ denotes the space gradient operator, V denotes the volume occupied by breast tissue, x denotes the space variable, $k_t(x)$, $\rho_t(x)$, and $c_t(x)$ are the thermal conductivity, density, and specific heat, respectively, of components like fat, tumor, cyst, skin or gland tissue in point x belonging to the sub-volume of V occupied by this component, ρ_b and c_b are the density (kg/m^3) and the specific heat of the blood (J/kg/K), respectively, ω_b is the blood perfusion rate (ml/s/mL), $Q_m(x)$ is the metabolic heat generation rate (W/m^3) of the tissue in
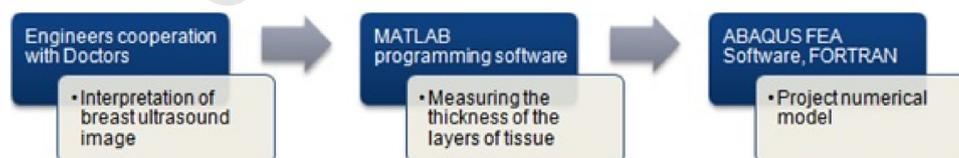
Fig. 1 – The methodology of breast numerical model development.
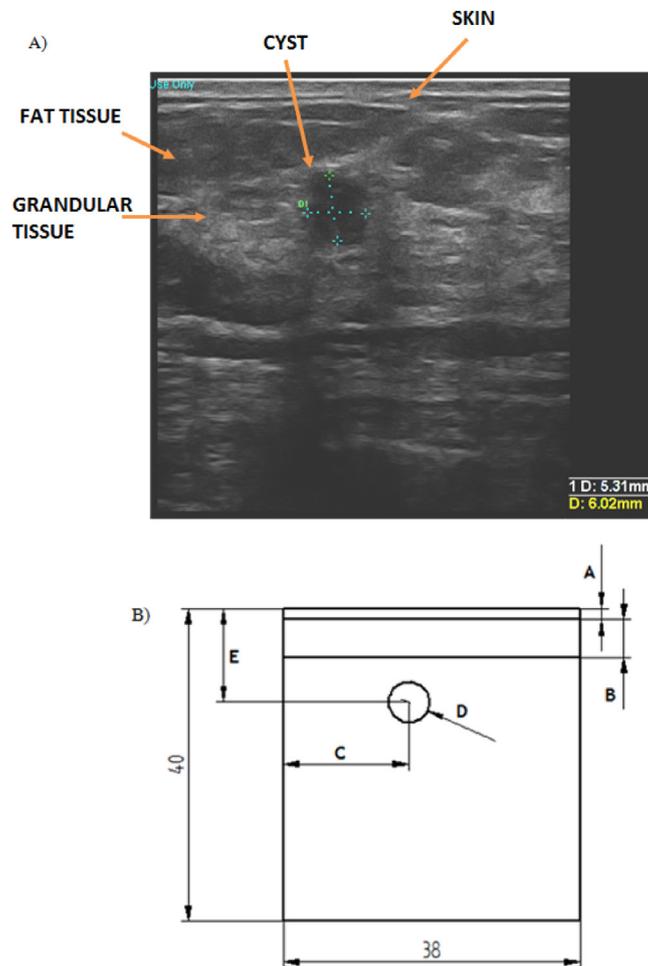
Fig. 2 – USG image and schematic diagram of the numerical model: A) USG data of a cancerous breast, B) simplified geometrical model of a breast where A denotes the thickness of the skin layer, B denotes the thickness of the fat layer, C and E denote the locations of the tumor or cyst in the breast gland, and D denotes the size of the tumor or cyst (Table 1, Table 2).

point x, T_b is the arterial blood temperature (°C) and T is the local temperature (°C) of the breast tissue.

The temperature of the arterial blood was approximated to be the core temperature of the body, 37 °C.

The initial temperature of the body and the arterial blood temperature was assumed to be equal to 37 °C. The external (ambient) temperature was assumed to be equal to 22 °C. To solve the bioheat Eq. (1), the Dirichlet boundary conditions were stated on the three internal walls of the breast scan (Fig. 4), where temperature T was assumed to be 37 °C (constant). On the ''skin'' wall, the Cauchy boundary condition (2) for the heat flux was stated. Then, the temperature of the "skin" wall was calculated after the solution of the heat transfer Eq. (1) was obtained.

The Cauchy boundary condition simulating heat transfer in the ''skin'' wall of the breast scan had the following form:

$$\boldsymbol{n} \cdot (k\nabla T) = h(T_z - T) + q_0, \qquad (2)$$

where $\boldsymbol{n}$ denotes the normal vector to the skin surface, q_0 is the heat flux density directed into the breast tissue that was

defined as equal to 0.0 $[\frac{W}{m^2}]$, h is the convective heat transfer coefficient taken as equal to 20.0 $[\frac{W}{m \cdot °C}]$, and T_z is the external temperature (ambient temperature) taken as equal to 22.0 °C.

The Cauchy boundary condition simulated heat dissipation through the breast skin surface due to temperature differences between the air and body temperatures. Table 3 contains the material properties used in the FEM numerical calculations.

3. Results

3.1. Healthy breasts

Based on the ultrasonography examination, the thickness of the fat tissue, the distance between the skin and abnormal tissue, and the cyst radius were presented in Tables 1 and 2.

The data were used to create a 2D numerical model as described above. A representative, numerically simulated color-coded temperature distribution in healthy breast tissue is presented in Fig. 5. It was observed that the temperature that occurred on the breast surface was lower than that in the
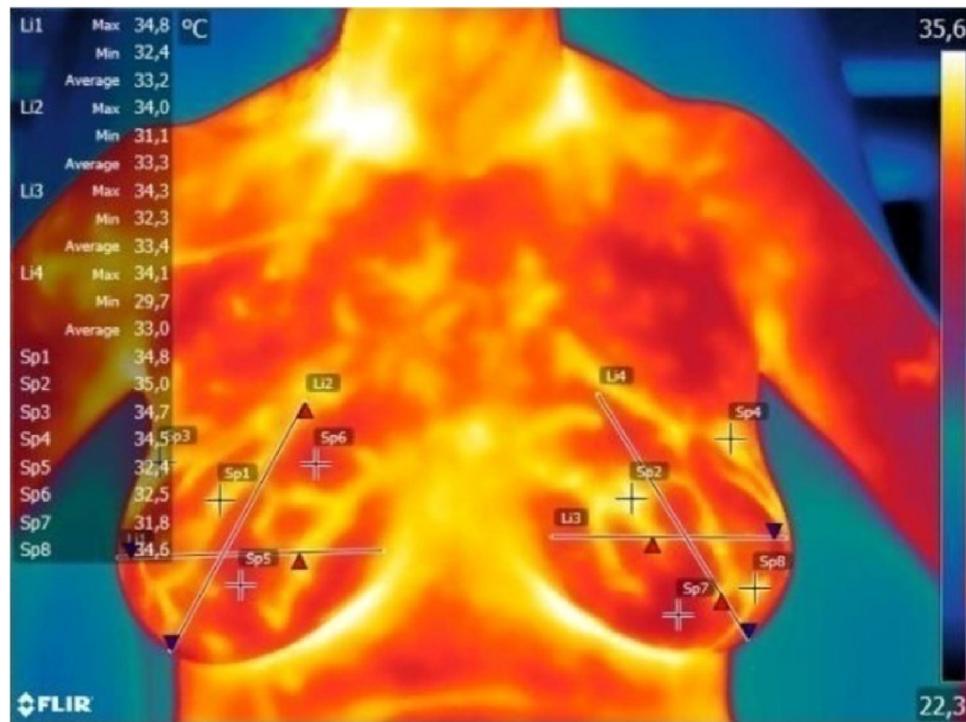
Fig. 3 – Temperature profiles of the breasts obtained by thermography.

breast's interior. The lowest temperature points were located in the top center of the symmetric model.

From the temperature maps obtained as thermographic images of the right and left healthy breasts [Fig.6], distribution asymmetry was not observed. The results obtained in the numerical simulation were compared with results obtained from the thermography in Table 4.

The mean temperature of the skin breast in thermography was calculated as a mean value from points obtained from thermographic images. The mean surface temperature of the skin in numerical simulations was calculated as the mean value on a 2 cm line lying in the center of the upper edge of the rectangle, i.e. of an idealized image of 2D USG. It enabled to partially eliminate the influence of the unreal boundary conditions stated on the side edges of the rectangle.

The highest temperature obtained by both methods had patient number 4, while the lowest temperature was observed in patient number 3, as described by Table 4. In Table 1, these patients were characterized by extreme values of the thickness of the fat layer. As the breast structure significantly varies among women, to determine whether the thickness of fat tissue, cyst radius, metabolism, or perfusion influenced the temperature distribution, additional simulations were performed.
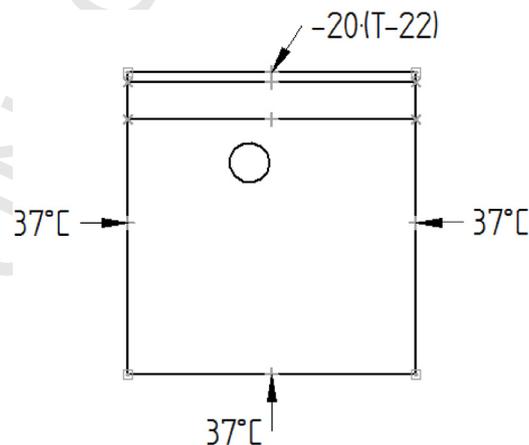
Fig. 4 – Diagram of boundary conditions during the modeling process.

Table 3 – Material properties. Data reproduced from [7,9,11,12,32].

Type of tissue	Density ρ [kg/m^3]	Thermal conductivity k [W/mK]	Specific heat c [J/kgK]	Metabolism Q [W/m^3]	Blood Perfusion Rate[ml/s/mL]
Skin	1,200.00	0.23	3,330.00	368.00	106.00
Fat	930.00	0.21	2,770.00	400.00	47.00
Gland	1,050.00	0.48	3,770.00	700.00	150.00
Cyst	1,000.00	0.56	4,200.00	0.00	0.00
Tumor	1,050.00	0.48	3,852.00	29,000.00÷58,000.00	10,000.00
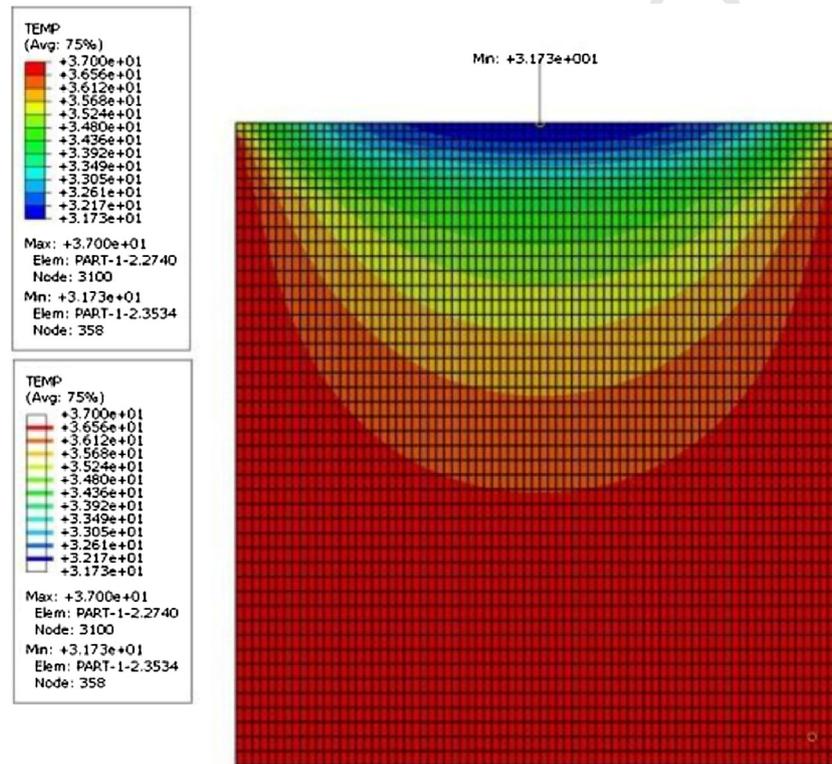
Fig. 5 – Results of numerical simulations of the average temperature distribution in the healthy breasts.

Fig. 7 shows that the temperature of the breast tissue slightly decreased by 1 °C when the thickness of fat tissue increased four times and by 1.4 °C when the thickness of fat tissue increased to 8 mm.

As can be seen from Fig. 8, the temperature on the skin decreased with an increase in the cyst radius. The decrease of temperature was T = 31.1 °C for the 8 mm cyst in comparison to the temperature measured at the surface of the breast without a cyst at T = 31.6 °C (0.4 °C lower). In Penne's equation, metabolism and blood perfusion were taken into account. Therefore, the influence of those parameters on the temperature distribution was analyzed. The metabolism and perfusion values were changed, while the thickness of the building tissue layers remained unchanged.

The data in Table 5 show that when the metabolism value increased by 40%, the temperature rose by 0.04 °C. Furthermore, it was observed that perfusion had a greater impact on the temperature distribution on the breast skin surface than metabolism. As can be seen, an increase in the metabolism rate by a factor of n = 2 induced a temperature increase of 0.09 °C, while an increase in the perfusion by a factor of n = 2 caused a temperature increase of 0.68 °C.

3.2. Cancerous breasts

The numerical simulation included two types of tumors, benign and malignant, and various rates of the heat transfer coefficient of the benign and malignant cancer. The benign cancer was defined by metabolic heat production equal to 29,000.00 W/m^2, and the malignant was defined by metabolic heat production of 58,000.00 W/m^2. In Fig. 9, the influence of the two different tumor types on the minimal values of the temperature on the skin surface for various tumor sizes is shown. Table 6 summarizes the dependencies of the minimal temperature of the breast surface on the tumor size, tumor malignancy, and tumor location, given here by the distance from the skin and percentage of fat quantum in the breast anatomy.

The exemplary effect of the heat transfer coefficient on the temperature distribution at the breast skin surface was presented. Five cases of tumor sizes from our data were
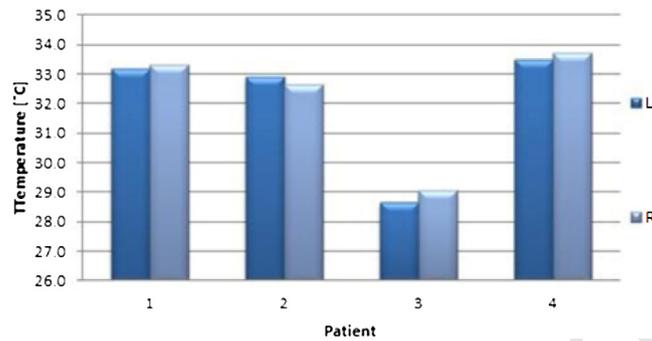
Fig. 6 – Mean temperature obtained from computational simulation; left healthy breast (L) and right healthy breast (R).

Table 4 – A comparison of the results obtained from the thermography and numerical model applied to both breasts' denotes a difference between the mean breast skin temperature obtained in the thermography and obtained in the numerical model.

Patient	Breast temperature obtained in thermography [³C]		Breast temperature obtained in the numerical model[³C]	ΔT [³C]	ΔT [³C]
	Left	Right		Left	Right
1	33.20	33.30	31.18	2.02	2.12
2	32.90	32.70	31.20	1.70	1.50
3	28.70	29.10	30.93	2.23	1.83
4	33.50	33.70	31.73	1.77	1.97
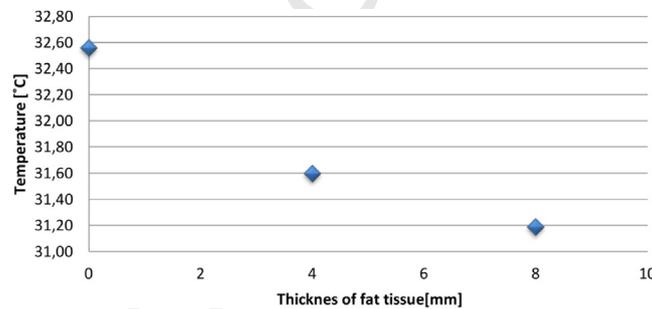
Fig. 7 – The minimum temperature of the breast surface as a function of fat tissue thickness.
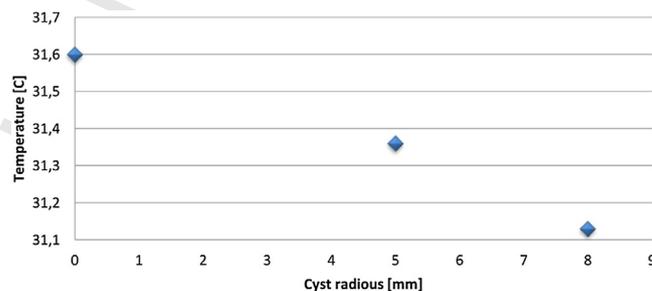
Fig. 8 – The minimum temperature of the breast surface as a function of cyst radius.

Table 5 – Temperature values obtained concerning metabolism (Qm) and perfusion changes.					
Q_m[W/m³]	T $_{Qm}$[³C]	ΔT $_{Qm}$[³C]	Perfusion [W/m³K]	Tp [³C]	ΔT p[³C]
500.00	32.56	0.00	496.00	32.29	0.00
700.00	32.60	0.04	900.00	31.85	0.44
1,000.00	32.65	0.09	1,800.00	31.17	1.12
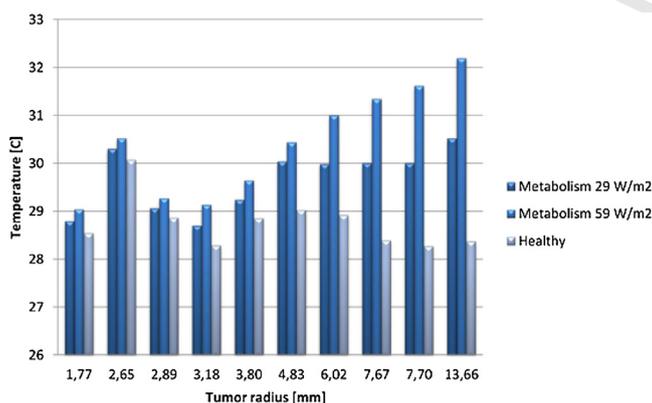
Fig. 9 – The minimal temperature of the breast surface depending on the tumor radius for two different metabolism rates. ''Healthy'' denotes the breast model with the same structural parameters but without a cancerous lesion.

Table 6 – The minimal temperature on the breast surface for given tumor size, distance from the skin layer, and malignancy with heat transfer coefficient equal to 20 W/mK.					
Model	Radius [mm]	The minimal temperature on the breast surface		Tumor distance from the skin layer [mm]	Morphology
		Metabolism: 29,000.00 W/m²	Metabolism: 59,000.00 W/m²		[%] fat quantum in breast anatomy
8	1.78	28.79	29.04	11.82	15.81
1	2.65	30.30	30.52	11.96	12.13
2	4.83	30.04	30.44	13.14	13.44
6	6.02	29.98	31.00	16.19	14.19
7	3.18	28.70	29.13	17.25	22.04
9	2.89	29.06	29.27	20.66	16.24
5	7.67	30.00	31.34	22.09	17.16
4	7.70	30.00	31.62	23.99	100.00
10	13.66	30.52	32.19	25.63	22.61
3	3.80	29.24	29.64	27.23	100.00

chosen, and the minimal skin temperature for two different tumor types is shown in Fig. 10 and Fig. 11 assuming the heat transfer coefficients values of 10 and 20 W/mK, respectively.

The simulation takes into account the type of cancer. The benign cancer was described by 29,000.00 W/m² of metabolic heat production and the malignant by 58,000.00 W/m².

4. Discussion

The simplified breast geometry model introduced above in a form without circular symmetry but based directly on the USG

scan was previously used to simulate the effects of ultrasonic hyperthermia in soft tissues in papers [37,38].

In the healthy breast study, no asymmetry between the left and right breasts in the measurements by the IRT temperature distribution breast maps was observed. These breasts were previously qualified by a medical doctor as healthy breasts. The average temperature obtained from the analysis of thermography data on the right and left breasts differed insignificantly by less than 0.4 °C, as proposed by Table 4. This confirmed that the four considered cases could be assumed as healthy breasts in agreement with the USG examination. As was noticed in the previous section the mean temperature of
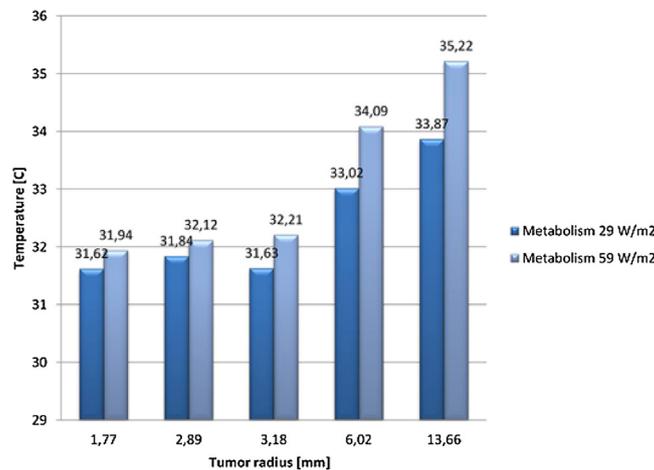
Fig. 10 – The minimum temperature on the surface of the breast for five selected numerical models. The parameter used in the simulation: the heat transfer coefficient equal to 10 W/mK. The simulation takes into account the type of cancer. The benign cancer was described by 29,000.00 W/m^2 of metabolic heat production and malignant by 58,000.00 W/m^2.
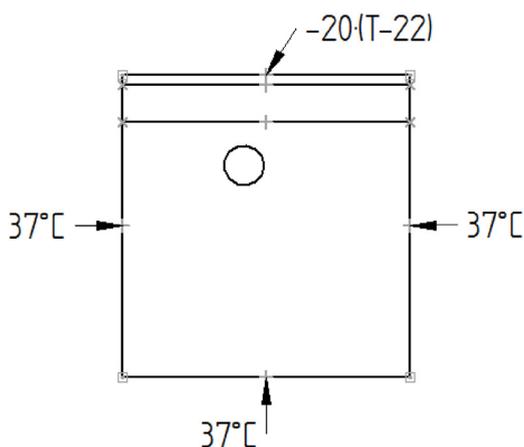
Fig. 11 The minimal temperature on the surface of the breast for five selected models. The parameter used in the simulation: the heat transfer coefficient equal to 20 W/mK.

the skin breast in thermography and numerical simulations were calculated not exactly from the same points lying on the breast skin. Besides, a constant temperature equal to the internal body temperature was assumed on the sides of the rectangle. It is clear that near the skin, this temperature is lower. Such a simplification in the boundary conditions assumed in the model leads to an increase in the value of the numerically calculated breast skin temperature. Additionally, in the numerical modeling of the healthy breasts in individual patients, we assumed the same geometry of left and right breast anatomy, see the same values of temperature for both breasts in Table 4. Besides, the same values in all cases for all thermal parameters of skin tissue, adipose tissue and glandular tissue, as well as metabolism and perfusion were used. The simplified boundary conditions in the assumed 2D

geometrical model of the breast together with non differentiated between patients' thermal tissue parameters are the main reason for differences between numerical and measured temperature values. The differences between mean breast skin temperature measured from thermography and numerical models were in the range of 1.7 °C–2.23 °C. Additionally, from Table 4, we observed that the highest temperature in both methods was obtained in patient number 4 while the lowest temperature was observed in patient number 3. Based on Table 1, these patients were characterized by the extreme values of the measured parameters. Patient 3 had the breast type P1 and the widest fat layer, whereas patient 4 had breast type N1 and the finest fat layer. The two others were classified by the same breast type of P2. Our analysis focuses on showing the differences between the values of temperature, i.e. on finding the tendency, not on the modeling of real values of the skin temperature. Summing up, the numerical model took into account changes in the geometric parameters like the layer's size of the adipose, glandular tissue, and skin tissue. These were the changes in between the breast anatomical structure of patients without taking into account differences in particular tissue physiology. We have shown that the breast type, adipose or glandular, influences measured skin temperature, which corresponds to the greater or smaller thickness of the adipose tissue layer in the numerical model. Fig. 7 shows that the temperature of the breasts obtained by numerical simulations slightly decreased by 1 °C when the thickness of the fat tissue increased from 0 to 4 mm, and by 1.4 °C when the thickness of the fat tissue increased from 4 to 8 mm. This result was in agreement with [13]. A cyst in the breast is a benign lesion, generally filled with fluid, characterized by the absence of a vascular system and low metabolism. The lack of perfusion and metabolism inside the cyst volume reduces the temperature on the surface of the breast proportionally to the cyst radius. It can be seen from Fig. 8 that the temperature on the skin decreased with an increase in the cyst radius, as confirmed in paper [39]. The decrease of temperature was T = 31.1 °C for the 8 mm cyst in comparison to the tempera-

ture measured at the surface of the breast without a cyst at T = 31.6 °C (0.4 °C lower).

By numerical simulation, we confirmed that for the normal breast the blood perfusion hada greater impact on temperature distribution' than heat sources connected with the tissue metabolism. These findings are in agreement with the results presented in many papers, e.g. [6] and [11,12]. We demonstrated in Table 5 that when the metabolism value was increased by 40%, the temperature rose by 0.04 °C. Furthermore, it was observed that perfusion had a greater impact on the temperature distribution on the breast skin surface. We calculated that an increase in the metabolism rate by a factor of n = 2 induced the temperature increase of the only 0.09 °C, while an increase in the perfusion by a factor of n = 2 caused the temperature to increase by 0.68 °C. The local tissue metabolism identified above in the numerical model as the volumetric heat source, in the case of cancerous tissue is related to the much faster metabolism in the neoplastic tissue than is expected in the normal breast. The value of metabolism, 20–40 times greater than in normal tissue, is proportional to the tumor growth rate and the degree of lesion malignancy. The intensity of metabolism is responsible for the power of heat sources. The value of heat flux transporting heat to the breast skin is also affected by the size of the lesion. It is determined by the volume of the lesion, as the total efficiency of heat sources is proportional to the heat power intensity and extent of the area of a given metabolism. Additionally, the tumor perfusion, even having the value greater than in normal surrounding tissue, it is not as efficient in removing heat as normal, uniform perfusion of healthy tissue due to chaotic, uneven growth of blood vessels, i.e. abnormal angiogenesis. In the simulation performed for cancerous breasts, cf. Table 6, the minimal temperature enabled us to confirm that the temperature of the breast surface is strongly connected to the location and morphology of breast cancer. The tumor radius between 1.75 and 3.50 mm had a significant effect on the temperature distribution on the skin of the part of the breast closest to the tumor location. In the early stages of carcinogenesis, lesions smaller than 3.50 mm in diameter, located farthest from the skin layer, are the most difficult to detect. The difference in the minimal temperature, measured at the surface of the healthy breast and the breast with a benign lesion with a 1.78 mm radius, was equal to 0.25 °C. For the same radius of a malignant lesion, the temperature on the skin surface was higher by 0.50 °C. The similar temperature distribution was obtained for a cancerous lesion with a radius of 3.18 mm, which confirmed that the temperature distribution on the surface of the breast also depends on the location of the tumor. For cancerous lesions over a 4.83 mm radius, the temperature average increased by 1.50 °C in comparison to the temperature distribution on the surface without connection to the location of the tumor. Furthermore, the result of the simulations confirmed the "damping" character of the fat layer, providing to decreasing the temperature of the breast's skin, similarly as in the healthy breasts. Tumors located in the breast area of the predominant fat gland were difficult to detect by changes in the skin temperature of the part of the breast closest to the tumor location (Table 6). It was shown that the temperature on the breast surface increased from 0.5 °C to 1.5 °C when the metabolic heat production was doubled (Fig. 10).

As shown in Fig. 9, tumor size had an evident influence on the temperature distribution on the breast surface. The temperature on the skin surface increased when the tumor radius increased (see results of [13]). As can be seen from Fig. 9, the temperature on the skin surface of a breast with a 1.77 mm malignant tumor radius was equal to 29.04 °C. For the malignant breast tumor with a 13.66 mm lesion radius, the temperature on the skin was equal to 32.19 °C. The temperature distribution on the breast skin differed for benign and malignant breast tumors. It was observed that the temperature was lower on the skin surface for breasts with benign cancer. An increase in skin surface temperature was also observed for benign cancer with an increased tumor radius. For the benign lesion with a 1.77 mm radius, the temperature on the surface was equal to 28.79 °C. A greater radius of benign tumors in the breast caused a higher temperature on the surface equal to 30.52 °C.

Two main factors in abnormal angiogenesis in cancer, a "braid" of vessels "entwining" the tumor, and the lack of normal vascular net responsible for heat transfer inside the tumor volume, change the thermal conductivity coefficient of cancerous tissue. But we did not consider the change in the thermal conductivity coefficient in the tumor itself compared to normal tissue due to the lack of available numerical data in the literature. We simulated only the change in the conductivity coefficient of the skin layers was simulated. Namely, the numerical simulation confirmed that the reduction of the skin heat conductivity coefficient caused an increase of the breast surface temperature of 1.0 °C–3.0 °C, depending on the lesion types inside the breast, a benign cancer lesion, and a malignant lesion. So it could be assumed that patients with a greater capacity for heat transfer by the skin will be easier to diagnose by the thermographic examination. The results confirmed the significant influence of the thermal properties of tissue, including the heat transfer coefficient on the temperature value of the breast skin surface.

5. Conclusions

We introduced a simplified 2D numerical model using ultrasound data for 14 women that allowed for a qualitative assessment of their breast condition. The aim of the study was not to construct a mathematical and numerical model for an individual patient to achieve compliance with the thermography reading. However, we have shown that thermography is suitable for certain comparative analyzes, in particular for the classification of the anatomical type of healthy breast. A simple numerical model, although a difference was obtained between the measured and calculated skin temperature value of healthy breasts, allowed to confirm the dependence of the breast skin temperature on the thickness of the tissue layers included in the model. We used a simplified numerical model to analyze the impact of the anatomical heterogeneous structure of the breasts, particularly the presence of cancer, on changes in the surface temperature of the breast skin.

The results we obtained for the healthy breasts were consistent with those obtained from the thermographic images. In detail, we concluded that the breast thermal condition is affected by the breast morphology, particularly

the percentage of fat in the breast tissue, the size of the tumor or cyst, its location relative to the skin surface, the malignancy degree of the tumor, and the thermal properties of the different breast tissues. We showed that increasing the thickness of the fat tissue causes a decrease in the temperature value on the surface of the skin. Furthermore, the greater impact of the blood perfusion rate variations on the breast surface temperature changes in comparison to metabolism heat changes was confirmed. Additionally, the measurable decrease in the surface temperature depending on the presence and size of the cyst was confirmed. The numerical simulations revealed that the differences in temperature distribution on the breast surface in the presence of cancer may differ between 0.5 °C and 3.0 °C in comparison to healthy breasts, which means that thermography should detect the existence of a cancerous lesion. These findings need more examination to find to what extent our simplified numerical model and the standard USG data we used as a clinical basis in the numerical model creation could help in assessing the usefulness of thermography in the diagnosis of breast cancer instead of the more sophisticated models with more advanced imaging techniques that are used now. In the end, we would like to repeat that to construct our very simplified model, we used USG data, collected from 10 patients and 4 volunteers, which is not common in publications on numerical modeling of thermal processes in the breast in the context of thermographic diagnostic assessment. The paper [40], published very recently in May 2020, which used clinical data (MRI of 11 patients) to assess thermography, also emphasizes the importance of results based on clinical data and the rarity of such scientific reports. We have not found any publications in the IRT assessment, that would directly use ultrasound clinical data to build a numerical model of cancerous breast heat transfer.

Author statement

All persons who meet authorship criteria are listed as authors, and all authors certify that they have participated sufficiently in the work to take public responsibility for the content, including participation in the concept, design, analysis, writing, or revision of the manuscript. Furthermore, each author certifies that this material or similar material has not been and will not be submitted to or published in any other publication before its appearance in the Journal of the Biocybernetics and Biomedical Engineering.

Acknowledgment

REFERENCES

[1] Burzynska M, Maniecka-Bryla I, Pikala M. Trends of mortality due to breast cancer in Poland, 2000-2016. BMC Public Health 2020;20:120.

[2] Brem RF, Lenihan MJ, Lieberman J, Torrente J. Screening breast ultrasound: past, present, and future. AJR Am J Roentgenol 2015;204(2):234–40.

[3] Nowikiewicz T, Nowak A, Wisniewska M, Wisniewski M, Nowikiewicz M, Zegarski W. Analysis of the causes of false negative and false positive results of preoperative axillary ultrasound in patients with early breast cancer - a single-centre study. Contemp Oncol (Pozn) 2018;22(4):247–51. http://dx.doi.org/10.5114/wo.2018.82644

[4] Suman S, Suman G, Mishra S. Current advances in breast cancer research: a molecular approach. Bentham Science Publishers; 2020 [chapter 2: sumam G, Patra A. Current imaging techniques in breast cancer: an overview]; 2020.

[5] Byra M, Dobruch-Sobczak K, Klimonda Z, Piotrzkowska-Wroblewska H, Litniewski J. Early prediction of response to neoadjuvant chemotherapy in breast cancer sonography using Siamese convolutional neural networks. IEEE J Biomed Health Inform 2020. http://dx.doi.org/10.1109/JBHI.2020.3008040

[6] Ng EYK, Ung LN, Ng FC, Sim LSJ. Statistical analysis of healthy and malignant breast thermography. J Med Eng Tech 2001;25(6):253–63.

[7] Ng EY, Sudharsan NM. An improved three-dimensional direct numerical modelling and thermal analysis of a female breast with tumour. Proc Inst Mech Eng H 2001;215(1):25–37.

[8] Ng EY, Sudharsan NM. Computer simulation in conjunction with medical thermography as an adjunct tool for early detection of breast cancer. BMC Cancer 2004;4:17.

[9] Ng EYK. A review of thermography as promising non-invasive detection modality for breast tumor. Int J Therm Sci 2009;48(5):849–59.

[10] Singh D, Singh AK. Role of image thermography in early breast cancer detection- Past, present and future. Comput Methods Programs Biomed 2020;183105074. http://dx.doi.org/10.1016/j.cmpb.2019.105074

[11] González FJ. Thermal simulation of breast tumors. Rev mexfis 2007;53(4):323–6.

[12] González FJ. Non-invasive estimation of the metabolic heat production of breast tumors using digital infrared imaging. Quant Infrared Thermogr J 2011;8(2):139–48.

[13] Kwok J, Krzyspiak J. Thermal imaging and analysis for breast tumor detection. BEE 4530: computer-Aided Engineering: applications to Biomedical Processes; 2007.

[14] Chanmugam A, Hatwar R, Herman C. Thermal analysis of cancerous breast model. Int Mech Eng Congress Expo 2012;2012:134–43.

[15] Mital M, Pidaparti RM. Breast tumor simulation and parameters estimation using evolutionary algorithms. Model SimulatEng 2008;2008:1–6.

[16] Ghayoumi Zadeh H, Haddadnia J, RahmaniSeryasat O, MostafaviIsfahani SM. Segmenting breast cancerous regions in thermal images using fuzzy active contours. EXCLI J 2016;15:532–50.

[17] Pennes HH. Analysis of tissue and arterial blood temperatures in the resting human forearm. J Appl Physiol 1998;85(1):5–34.

[18] Figueiredo AAA, do Nascimento JG, Malheiros FC, da Silva Ignacio LH, Fernandes HC, Guimaraes G. Breast tumor localization using skin surface temperatures from a 2D anatomic model without knowledge of the thermophysical properties. Comput Methods Programs Biomed 2019;172:65–77.

[19] Gonçalves CB, Leles ACQ, Oliveira LE, Guimaraes G, Cunha JR, Fernandes H. Machine learning and infrared thermography for breast Cancer detection. Proceedings 2019;27(1):45.

[20] Singh D, Singh A. Role of image thermography in early breast Cancer detection- past, present and future. Comput Meth Prog Bio 2019;183105074.

[21] Abdel-Nasser M, Moreno A, Puig D. Breast Cancer detection in thermal infrared images using representation learning and texture analysis methods. Electronics 2019;8(1):100.

[22] Dua G, Mulaveesala R. Applicability of active infrared thermography for screening of human breast: a numerical study. J Biomed Opt 2018;23(3):1–9.

[23] Chanmugam A, Hatwar R, Herman C. Thermal analysis of cancerous breast model. Proceedings of ASME 2012 IMECE; 2012.

[24] Bakker JF, Paulides MM, Obdeijn IM, van Rhoon GC, van Dongen KW. An ultrasound cylindrical phased array for deep heating in the breast: theoretical design using heterogeneous models. Phys Med Biol 2009;54(10):3201–15.

[25] Okita K, Narumi R, Azuma T, Furusawa H, Shidooka J, Takagi S, et al. Effects of breast structure on high-intensity focused ultrasound focal error. J Ther Ultrasound 2018;6:4.

[26] de Holanda AA, Gonçalves AK, de Medeiros RD, de Oliveira AM, Maranhão TM. Ultrasound findings of the physiological changes and most common breast diseases during pregnancy and lactation. Radiol Bras 2016;49(6):389–96.

[27] Wang L. Early diagnosis of breast Cancer. Sensors 2017;17(7):1572.

[28] Paruch M. Mathematical modeling of breast tumor destruction using fast heating during radiofrequency ablation. Materials 2019;13(1):136.

[29] Manohar S, Dantuma M. Current and future trends in photoacoustic breast imaging. Photoacoustic 2019;16100134.

[30] Bezerra LA, Ribeiro RR, Lyra PRM, Lima RCF. An empirical correlation to estimate thermal properties of the breast and of the breast nodule using thermographic images and optimization techniques. Int J Heat Mass Transf 2020;149119215.

[31] Gambin B, Kruglenko E, Wójcik J. Relationship between thermal and ultrasound fields in breast tissue in vivo. Hydroacoustics 2015;18:53–8.

[32] Gambin B, Byra M, Kruglenko E, Doubrovina O, Nowicki A. Ultrasonic measurement of temperature rise in breast cyst and in neighboring tissues as a method of tissue differentiation. Arch Acoust 2016;41(4):791–8.

[33] Jakubowski W, Dobruch-Sobczak K, Migda D. Standards of the polish ultrasound society – update. Sonomammography examination. JUltrason 2012;12(50):245–61. DOI:10.15557/JoU.2012.0010.

[34] Wolfe JN. Risk for breast cancer development determined by mammographic parenchymal pattern. Cancer 1976;37(5):2486–92.

[35] Piotrzkowska-Wróblewska H, Dobruch-Sobczak K, Byra M, Nowicki A. Open access database of raw ultrasonic signals acquired from malignant and benign breast lesions. Med Phys 2017;44(11):6105–9. http://dx.doi.org/10.1002/mp.12538

[36] Popiela TJ, C´wierz A, Pypkowska A, Trzyna M. Atlas termograficzny: rak Piersi. Warszawa: Wydawnictwo Lekarskie PZWL; 2015.

[37] Gambin B, Kujawska T, Kruglenko E, Mizera A, Nowicki A. Temperature fields induced by low power focused ultrasound during gene therapy. Numerical predictions and experimental results. Arch Acoust 2009;34(4):445–60.

[38] Gambin B, Kruglenko E, Kujawska T, Michajlow M. Modeling of tissues in vivo heating induced by exposure to therapeutic ultrasound. Acta Phys Pol A 2011;119(6):950–6.

[39] Balusu K, Suganthi SS, Ramakrishnan S. Modelling bio-heat transfer in breast cysts using finite element analysis.2014 International Conference on Informatics, Electronics & Vision (ICIEV), Dhaka; 2014;1–4. http://dx.doi.org/10.1109/ICIEV.2014.6850842

[40] Lozano A, Hayes JC, Compton LM, et al. Determining the thermal characteristics of breast cancer based on high-resolution infrared imaging, 3D breast scans, and magnetic resonance imaging. Sci Rep 2020;10(10105). doi.org/10.1038/s41598-020-66926-6.